Short-range Forecasting Research

Short Range Forecasting Division
Scientific Paper No. 13

A Balanced Ocean Model with Outcropping

by
Paul Cloke
and
M.J.P. Cullen

August 1992

Meteorological Office
London Road
Bracknell
Berkshire
RG12 2SZ
United Kingdom

Short Range Forecasting Research

Scientific Paper No. 13

A Balanced Ocean Model with Outcropping

by

Paul Cloke

and

M.J.P.Cullen

August 1992

Short Range Forecasting Research
Meteorological Office
London Road
Bracknell
Berkshire RG12 2SZ
ENGLAND

N.B This paper has not been published.Permission to quote from it must be obtained from the above Met. Office branch.

Abstract

A numerical model is presented. The model represents a single shallow water layer of constant density. The model is based upon the geostrophic momentum approximation (GM) equations, an equation set which does not support gravity waves. The GM equations are intermediate in accuracy between the quasi-geostrophic (QG) equations and the shallow water equations. In contrast to the more common QG equations the GM set is valid for large layer thickness perturbations. The GM set also has the advantage over many other balanced sets in applying the exact kinematic boundary condition of no normal flow at solid walls rather than imposing conditions such as no normal geostrophic flow, which is an error of order Rossby number.

The model we describe is based around a predictor-corrector approach. It is first developed and tested for cases with strictly positive layer thickness. The model is then modified to cope with zero layer thickness ('outcropping'). A flux limiting scheme is used to prevent regions of negative mass from being formed.

The model is compared with the analytic solutions of Parsons(1969) and the numerical solutions of Bogue, Huang and Bryan(1986). Good agreement is observed. Finally the model is used to look at a situation where both inertia and outcropping are important.

1 Introduction

A major deficiency of many previous idealised ocean models has been their neglect of non-linearities in either (or both) the momentum equations or the continuity equation. For example the quasi-geostrophic equations include inertial non-linearity, but ignore much of the non-linearity associated with change in isopycnal layer thickness. Much recent interest has been shown in intermediate models (*e.g.* Gent and McWilliams 1983, Allen *et al.* 1990) which remedy this difficulty by choosing a balance intermediate between quasi-geostrophic equations and the primitive equations while using a better approximation to the continuity equation.

In this paper the shallow water form of the geostrophic momentum approximation equations (Eliassen 1948) is used as a basis for a numerical ocean model. These equations have the properties of retaining most of the non-linearity in the momentum equations while including all of the non-linearity in the continuity equation. They also do not support gravity waves. The shallow water form is a prototype for a many layer isopycnal model (Bleck and Boudra 1986). The model is intended for, though not restricted to, highly idealised studies of a rectangular ocean on a beta plane. The technique can be applied to many other balanced equation sets. The model we describe is capable of modelling the outcropping of density surfaces, as occurs when the thickness of the shallow water layer becomes vanishingly small.

Allen *et al.*(1990) and Barth *et al.*(1990) have recently evaluated many intermediate models in both analytic and numerical situations. They plotted the Rossby number against error (the difference between the balanced solution and the solution to the primitive equations). In the specific cases they studied the geostrophic momentum equations perform relatively poorly. But they did note that the accuracy of the geostrophic momentum approximation was mostly unchanged as layer thickness variations increased, whereas many of the other intermediate models performed increasingly badly. The geostrophic momentum equations differ from most other balanced models studied by Allen *at al.* and Barth *et al.* in relying only the smallness of the Lagrangian Rossby number, in some cases this can differ greatly

from the Eulerian Rossby number which is required to be small for other balanced models. This suggests that the Eulerian Rossby number used in the studies of Allen *at al.* and Barth *et al.* is not necessarily the most important parameter in studying the accuracy of balanced models, other choices are clearly possible.

We consider the geostrophic momentum equations to be an interesting set to integrate not least because of the unambiguous way in which the boundary conditions are applied. Many other sets of intermediate models require the kinematic boundary condition to be partitioned between either the geostrophic and ageostrophic flow or between the rotational and divergent flow (*e.g.* McWilliams *et al.* 1990). The frequently used boundary conditions of imposing both streamfunction and velocity potential to be constant is an order Rossby number error. Much of our ultimate interest is in solutions where the layer thickness varies greatly over the basin. The boundary conditions are vital in these situations. The geostrophic momentum approximation formulation used here imposes the exact kinematic boundary condition of no normal flow at solid walls.

The geostrophic momentum equations are also one of the few intermediate sets of equations with conservation laws for energy, vorticity and potential enstrophy on an f-plane. Others being Salmon's balanced equations, Salmon (1983) and three forms of the semi-geostrophic equations which in the limit of constant f are the same as the geostrophic momentum equations(Salmon 1985,Shutts 1989 and Magnusdottir *et al.* 1990). Moreover existence and uniqueness proofs (Cullen and Purser 1989) and the many properties of the differential equations on an f plane make the set well posed and mathematically tractable.

In this paper we present a finite difference numerical model of the ocean based upon the shallow water form of the geostrophic momentum equations. The model can cope with the shallow water layer disappearing and is a one layer version of a multi-layer isopycnal ocean model. This paper describes the model formulation and verification. Future papers will apply this model to study new physical situations.

1.1 The Geostrophic Momentum Approximation

The geostrophic momentum approximation was first introduced by Eliassen(1948). Hoskins(1975) derived these equations calling them, in suitably transformed coordinates, the semi-geostrophic equations. These equations are obtained by replacing the full momentum in the horizontal momentum equations by the geostrophic momentum. The equations, in shallow water form, are

$$\frac{Du_g}{Dt} - fv + fv_g = 0, \tag{1}$$

$$\frac{Dv_g}{Dt} + fu - fu_g = 0, \tag{2}$$

where the pressure gradients have been replaced with geostrophic velocities given by,

$$fv_g = g' \frac{\partial h}{\partial x}, \tag{3}$$

$$-fu_g = g' \frac{\partial h}{\partial y}. \tag{4}$$

where f is allowed to vary and g' is the reduced gravity. The shallow water continuity equation is

$$\frac{Dh}{Dt} + h\nabla \cdot \underline{v} = 0. \tag{5}$$

for a layer of constant density and thickness h. Where

$$\frac{D}{Dt} = \frac{\partial}{\partial t} + u\frac{\partial}{\partial x} + v\frac{\partial}{\partial y}. \tag{6}$$

The geostrophic momentum approximation is obtained in the limit where the Lagrangian Rossby number is small, that is

$$\frac{\left|\frac{D}{Dt}\left(\frac{1}{f}\frac{Du}{Dt}\right)\right|}{|fu|} \ll 1, \tag{7}$$

and

$$\frac{\left|\frac{D}{Dt}\left(\frac{1}{f}\frac{Dv}{Dt}\right)\right|}{|fv|} \ll 1. \tag{8}$$

see Hoskins (1975)

These conditions are atypical for balanced models, which normally require small Eulerian Rossby number (*e.g.* McWilliams and Gent 1980). The accuracy of these equations is independent of the stratification. The more common quasi-geostrophic equations linearise about about a layer thickness, this is not necessary here. These equations are hence capable of representing isopycnal surfacing and separation processes such as occur in the Gulf Stream.

These equations have the following useful properties.

- They conserve analogues of potential vorticity and potential enstrophy for an f-plane.
- They conserve energy.
- Boundary conditions can be applied at solid boundaries in a natural manner.
- They have the full continuity equation for a single shallow. water layer of constant density ρ. This allows us to study situations allowing outcropping.
- They have existence and uniqueness proofs for an f-plane (Cullen and Purser 1989). No diffusion is required to close these equations.
- They can be derived from the Hamiltonian (Salmon 1985).
- They do not support gravity waves.

The equations will be integrated forward on a beta plane. A consequence of the variable Coriolis parameter, is that there is no vorticity conservation law for these equations, hence we cannot use the semi-geostrophic coordinate transform of Hoskins(1975).

We instead choose a predictor-corrector approach similar to that used by (Cullen 1989a) to integrate the momentum, continuity and geostrophic balance equations forward in time. We note that this technique can be applied to many other balanced sets, with minimal difficulty. Other authors (Salmon 1985, Shutts 1989, Magnusdottir and Schubert 1990) have introduced semi-geostrophic equations which, in the

limit of constant f, are the geostrophic momentum equations but which maintain conservation laws for both vorticity and energy in the case of a variable Coriolis parameter. In particular the approach used here to solve our equations could very simply be modified to solve Shutts equations. We have chosen to solve the geostrophic momentum equations because of their close resemblance to the shallow water form of the primitive equations and their ability to model outcropping without the gravity waves of other models.

2 Integration of the Semi-Geostrophic Equations

The equations are to be solved in a square basin with a prescribed wind forcing distributed over the thickness of the layer. The momentum sink is of linear drag form acting upon the geostrophic velocity only. This closes the energy equation and represents dissipation by vertical shearing of horizontal velocities. This formulation is used to guarantee that the drag always acts to reduce the energy (Cullen 1989b).

In this paper we look at a sub-tropical gyre representing the north Atlantic. Various values of stratification, wind and the Coriolis parameter are studied.

Before we describe the solution technique, it is useful to write the equations in non-dimensional form. The semi-geostrophic equations (1-6) are first written in mass transport form (*i.e.* where eqs. 1 and 2 are multiplied by h and the velocity $\underline{v}$ substituted by the mass transport $\underline{V} = \underline{v}h$). Our numerical model is formulated using mass transport as a prognostic variable. Source terms representing the wind and linear drag friction are then introduced into the x and y momentum equations respectively as $(\tau_x - \epsilon u_g)$ and $(\tau_y - \epsilon v_g)$. With this form of dissipation only one boundary condition (no flow through walls) is required at the basin edge. No condition is required on the tangential flow.

Scales are specified for $\underline{V}$,$\underline{v}_g$,h,t,$\underline{x}$ and f as $(v_0 h_0)$,v_0,h_0,f_0^{-1},L and f_0 respectively. The geostrophic momentum approximation equations in non-dimensional variables

become

$$h\frac{\partial u_g}{\partial t} + R_o U\frac{\partial u_g}{\partial x} + R_o V\frac{\partial u_g}{\partial y} - f'V + f'v_g h = \tau_M \tau'_x - \epsilon' u_g \tag{9}$$

$$h\frac{\partial v_g}{\partial t} + R_o U\frac{\partial v_g}{\partial x} + R_o V\frac{\partial v_g}{\partial y} + f'U - f'u_g h = \tau_M \tau'_y - \epsilon' v_g \tag{10}$$

$$\frac{\partial h}{\partial t} + R_o\left(\frac{\partial U}{\partial x} + \frac{\partial V}{\partial y}\right) = 0 \tag{11}$$

$$R_o f' v_g = B_u \frac{\partial h}{\partial x} \tag{12}$$

$$-R_o f' u_g = B_u \frac{\partial h}{\partial y} \tag{13}$$

where

$$R_o = \frac{v_0}{f_0 L}, \tag{14}$$

is the Rossby number and

$$B_u = \frac{g' h_0}{f_0^2 L^2}, \tag{15}$$

is the Burger number, a measure of the stratification. The number

$$\epsilon' = \frac{\epsilon}{f_0 h_0} \tag{16}$$

is the non-dimensional coefficient of linear drag, wind forcing is non-dimensionalised using

$$\tau_M \tau'_x = \frac{1}{f_0 v_0 h_0}\tau_x(x,y) \tag{17}$$

$$\tau_M \tau'_y = \frac{1}{f_0 v_0 h_0}\tau_y(x,y) \tag{18}$$

where $\tau_x(x,y)$ and $\tau_y(x,y)$ are the dimensional wind stresses, τ_M is a constant and τ'_x and τ'_y are order one functions of space (and time if required).

Choosing $f_0 = \beta L$ to help the physical interpretation of non-dimensional parameters gives $f' = \gamma + y'$ where $\gamma = f_{REF}/\beta L$, a measure of the variation of f over the basin, y' is the non-dimensional latitude and f_{REF} is f where $y' = 0$. This choice of f_0 also leads to $R_o = (L_I/L)^2$, $B_u = (L_\rho/\gamma L)^2$ and $\epsilon' = L_\epsilon/L$ where L_I, L_ρ, L_ϵ and L are the inertial length scale ($= (v_0/\beta)^{1/2}$), the Rossby radius ($= \sqrt{gh_0}/f_{REF}$), the scale of a frictional boundary current ($= \epsilon/\beta h_0$) and the length of the basin respectively.

We choose to scale the velocity using the maximum Sverdrup transport, for the wind stress ($\tau_x = -\tau_0 \cos(\pi y/L), \tau_y = 0$) then

$$\beta v_0 h_0 \sim \frac{\pi \tau_0}{L} \tag{19}$$

and

$$\tau_M \tau_x' = -\frac{1}{\pi} \cos(\pi y') \tag{20}$$

2.1 The Finite Difference Equations

Here we present the finite difference equations to be solved, the grid they are to be solved upon and the boundary conditions they have.

The variables are arranged on the grid (fig. 1) which has (N_X) h points in the x direction and (N_Y) h points in the y direction. The grid lengths in the x and y direction are Δx and Δy respectively such that $\Delta x = 1/(N_X)$ and $\Delta y = 1/(N_Y)$. The mass transport is calculated on an Arakawa 'C' grid (Arakawa, 1972), and the geostrophic velocities on the Arakawa 'D' grid. This choice has the advantage of representing redistribution of mass accurately while being a natural grid for the evaluation of geostrophic pressure gradients, although it has the disadvantage of averaging the pressure gradient terms of the momentum equations.

The discretised variables will be denoted by $A^n_{i,j}$ which is the value of the variable A at the ith grid point in the x direction and the jth grid point in the y direction at the time $n\Delta t$ where Δt is the time step. We define the usual delta and bar finite difference operators

$$\delta_x A = \frac{(A_{i+1/2,j} - A_{i-1/2,j})}{\Delta x} \tag{21}$$

and

$$\overline{A}^x = \frac{A_{i+1/2,j} + A_{i-1/2,j}}{2} \tag{22}$$

with the obvious equivalents in the y direction and $\delta_{2x} A$ being the equivalent of $\delta_x A$ over 2 grid lengths. Variables with no time labels are assumed to be at time level n. The time scheme we use is an Euler step for the first time step followed by a leapfrog scheme for all subsequent steps. An Asselin-Robert time filter (Asselin

1972,Robert 1966) is used at the end of each step on u_g v_g and h to remove the computational modes of the leapfrog scheme. The non-linear (advection) terms are written in a quadratic conservative form so that momentum($h\underline{u}_g$) is changed by a flux type equation and the friction term is calculated from values at the new time step. This is to enhance numerical stability especially as h approaches zero. The finite difference equations we solve are

$$\overline{h}^y\left(\frac{u_g^{n+1}-u_g^{n-1}}{2\Delta t}\right)+R_o\overline{\overline{U}^y\delta_x u_g}^x+V(R_o\delta_{2y}u_g-f')+\overline{\overline{f'v_g}^{xy}\overline{h}^y}^y=-\epsilon' u_g^{n+1}+\tau_M\tau_x' \quad (23)$$

$$\overline{h}^x\left(\frac{v_g^{n+1}-v_g^{n-1}}{2\Delta t}\right)+U(R_o\delta_{2x}v_g+f')+R_o\overline{\overline{V}^x\delta_y v_g}^y-\overline{\overline{fu_g}^{xy}\overline{h}^x}^y=-\epsilon' v_g^{n+1}+\tau_M\tau_y' \quad (24)$$

$$\left(\frac{h^{n+1}-h^{n-1}}{2\Delta t}\right)+R_o(\delta_x U+\delta_y V)=0 \quad (25)$$

$$-R_o f'v_g+B_u\delta_x h=0 \quad (26)$$

$$R_o f'u_g+B_u\delta_y h=0 \quad (27)$$

So that eqs. (23) and (27) are evaluated at u_g points on the grid, (24) and (26) are evaluated at v_g points and (25) is evaluated at h points.

2.1.1 Boundary Conditions

The boundary conditions are that there is no mass flux through the wall. This is a significant advantage over many other balanced models which either impose conditions on the geostrophic velocity at the boundary (*e.g.* the quasi-geostrophic equations impose $\underline{v}_g.\hat{n}=0$) or false conditions upon the divergent or non-divergent parts of the flow (*e.g.* McWilliams *et al.* 1990 who impose both streamfunction and velocity potential as zero). These alternative boundary conditions are often in error at order Rossby number. This becomes especially important as the layer thickness variation increase.

2.2 Solving the Finite Difference Equations

The technique used to solve these equations is somewhat similar to that used to solve the Navier-Stokes equations, where the pressure is corrected to ensure that the

velocity divergence is zero at the new time step (Williams 1969). Here, following Cullen (1989a), we correct the full mass transports to enforce geostrophic balance between the pressure and geostrophic velocities at the new time level. The eqs. (23-27) form a closed set of 3 prognostic and 2 diagnostic finite difference equations in five variables. The 3 prognostic equations give new values of u_g, v_g and h. But there is no prognostic equation for new values of the full mass transports U and V. Therefore an implicit equation has to be solved, at some point in the procedure, for the new values of these variables. The values of U and V required are those which make the prognostically calculated variables u_g, v_g and h satisfy the 2 diagnostic definitions of geostrophic balance, eqs.(26) and (27), at the end of the time step.

This numerical scheme, works in two stages, first ensuring that v_g and $\delta_x h$ satisfy eq.(26) by adjusting U and then by ensuring that u_g and $\delta_y h$ satisfy eqn. (27) by adjusting V and repeating until satisfactory convergence is obtained.

The scheme is similar to solving equations (23 –27) by alternating direction implicit (ADI) methods or by line relaxation in the Gauss-Seidel approach. To demonstrate the technique we describe one iteration.

2.2.1 The Evaluation of U

Evaluation of U consists of making a guess for v_g and h using values from the previous time steps, and finding the small changes in U which would enforce geostrophy in these new fields if v_g and h were recalculated using eqs.(24 and 25).

At the end of the previous time step (n) all the fields $(u_g^n, v_g^n, h^n, U$ and $V)$ are known and the diagnostic relations (26 and 27) have been satisfied by these geostrophic velocities and layer thickness fields. These variables and the ones from the previous time step $(n-1)$ are then used in (24 and 25) to get trial values of v_g and h at the new time level $(n+1)$. These values will be denoted here by $v_g^\#$ and $h^\#$. This trial step can be written

$$\overline{h}^x \left(\frac{v_g^\# - v_g^{n-1}}{2\Delta t} \right) + U(R_o \delta_{2x} v_g + f') + R_o \overline{\overline{V}^x \delta_y v_g}^y - \overline{f' u_g}^{xy} \overline{h}^x = -\epsilon' v_g^\# + \tau_M \tau_y' \quad (28)$$

$$\left(\frac{h^{\#} - h^{n-1}}{2\Delta t}\right) + R_o(\delta_x U + \delta_y V) = 0 \tag{29}$$

At boundaries we do not integrate for the geostrophic flow parallel to the wall so that where $U = 0$, v_g is not calculated and at a wall where $V = 0$, u_g is not calculated. Where boundary values of u_g and v_g are needed to evaluate the non-linear terms in the momentum eqs. (23 and 24) they are linearly extrapolated from the interior values. This is equivalent to side differencing.

Since the mass transports (U, V) are from the previous time step (or iteration) it can be seen that in general the values given by (28) and (29) do not satisfy the geostrophic balance relation (27). Namely

$$-R_o f' v_g^{\#} + B_u \delta_x h^{\#} = -R_1 \neq 0 \tag{30}$$

Where R_1 is known as the residual and is evaluated at v_g points on the grid (fig. 1). The task now is to find the small changes to U so that if this step is redone R_1 is zero.

For a given change in the mass transport (δU),the change in the result of the prognostic steps (28-29) is given by linearisation. This results in

$$\left(\frac{\overline{h^x}}{2\Delta t} + \epsilon'\right)\delta v_g + \delta U(R_o \delta_{2x} v_g + f') = 0 \tag{31}$$

$$\left(\frac{\delta h}{2\Delta t}\right) + R_o \delta_x \delta U = 0 \tag{32}$$

where δv_g and δh are the differences between the $\#$ values and the values obtained if U was changed by δU. We require that this δU should lead to the removal of the residuals R_1 in Eq. (30). Hence

$$-R_o f'(v_g^{\#} + \delta v_g) + B_u \delta_x (h^{\#} + \delta h) = 0 \tag{33}$$

Subtracting (30) from this leads to

$$-R_o f' \delta v_g + B_u \delta_x (\delta h) = R_1 \tag{34}$$

The 3 linear equations (31,32 and 34) for the 3 unknowns ($\delta U, \delta v_g$ and δh) can be solved given the correct boundary conditions ($\delta U = 0$ at east and west walls). These are combined to give

$$\frac{\delta h}{2\Delta t} + \delta_x \left[\frac{(R_1 - B_u \delta_x(\delta h))}{f'(f' + R_o \delta_{2x} v_g)} \left(\frac{\overline{h}^x}{2\Delta t} + \epsilon' \right) \right] = 0 \tag{35}$$

which is N_Y tridiagonal matrix inversions each for the N_X δh values of a row. Elimination of δv_g between Eq.(31) and (34) gives

$$R_o \delta U = \frac{(R_1 - B_u \delta_x(\delta h))}{f'(f' + R_o \delta_{2x} v_g)} \left(\frac{\overline{h}^x}{2\Delta t} + \epsilon' \right) \tag{36}$$

which relates δU with δh and other quantities known after the predictor stage. The solution δh from (35) is substituted back into eq.(36) to obtain δU which is then added onto U.

The evaluation of V follows a similar procedure. We solve

$$\frac{\delta h}{2\Delta t} + \delta_y \left[\frac{(R_2 - B_u \delta_y(\delta h))}{f'(f' - R_o \delta_{2y} u_g)} \left(\frac{\overline{h}^y}{2\Delta t} + \epsilon' \right) \right] = 0 \tag{37}$$

where $R_2 = -R_o f u_g^{\#} - B_u \delta_y h^{\#}$ This is N_X tridiagonal matrix inversions each for the N_Y δh values of a column. The equation relating δh and δV is

$$R_o \delta V = \frac{(R_2 - B_u \delta_y(\delta h))}{f'(f' - R_o \delta_{2y} u_g)} \left(\frac{\overline{h}^y}{2\Delta t} + \epsilon' \right) \tag{38}$$

The correction δh from eq.(37) is inserted into eq.(38) to obtain δV and hence the new V.

The loop of doing trial steps for v_g and h and correcting U to satisfy geostrophy followed by doing trial steps for u_g and h and correcting V to satisfy geostrophy, is repeated until the residuals R_1 and R_2 are sufficiently small (see fig. 2). If the residuals were exactly zero then we would have precisely solved the finite difference equations(23–27). We then proceed to the next step.

The iteration is necessary because updated values of mass transport have not been included in the perpendicular direction. After evaluating a new V using eq.(37) and (38) reevaluation of eqs. (28) and (29) will result in the residual R_1 in eq.(30) not

being zero. After the final iteration, all predictor steps are redone to include the latest and best values of mass transport. Each tridiagonal matrix inversions requires only order N calculations for problem of length N.

This method of solution can be very cheap although if a high level of convergence is not obtained, the spin-up process may be slowed down (Cloke 1992). An alternative method that can solve these equations very accurately is to solve for δU and δV simultaneously. This requires a variable coefficient elliptic inversion for the δh's. This is much more expensive than the tridiagonal inversion approach we use here. One elliptic inversion takes a minimum of $N \log N$ calculations for an N gridpoint domain, whereas the tridiagonal inversions we require here are accomplished in order N calculations. In this paper only steady solutions are examined and so an error in the spin-up scale is unimportant.

The tridiagonal inversions (35, 37) can be solved as long as

$$(f' - R_o \delta_{2y} u_g)^n \neq 0 \tag{39}$$

and

$$(f' + R_o \delta_{2x} v_g)^n \neq 0 \tag{40}$$

at all h points. The full algorithm is shown in fig. (2)

3 Model Runs

Here we look at solutions from the model. In the limit of very large mean depth compared to layer thickness variations, the shallow water continuity equation tends to the non-divergent equation. For idealised wind forcing, solutions similar to those of Veronis(1966) are expected. Figures (4–5) show some solutions where the layer thickness varies very little from the mean and the wind forcing has the dimensional form ($\tau_x = -0.5 * \tau_0 \sin(\pi x/L)\cos(\pi y/L), \tau_y = 0.5 * \tau_0 \cos(\pi x/L)\sin(\pi y/L)$). We show both the layer thickness and the streamfunction. The streamfunction is derived by noting that the mass transport is non-divergent in the steady state (from eq. 11). This is true even if the layer thickness varies greatly.

The geostrophic flow cannot cross layer thickness contours and the mass transport cannot cross streamlines. Figures (4 and 5) show the layer thickness and streamfunction in the case of very small Rossby number(table 1, fig.17 shows the non-dimensional parameters). In this regime the momentum equations(9 and 10) become linear, and the classic Stommel(1948) gyre is reproduced. A marked difference between streamlines and layer thickness contours is obtained. The streamlines do not intersect the walls whereas the layer thickness contours hit the wall. This is because of the different boundary conditions on these fields. The streamfunction is zero at the walls and the layer thickness satisfies a balance between the geostrophic flow the Ekman terms and the friction. On the northern wall, for example, this is

$$\frac{1}{2}\frac{B_u}{R_o}\frac{\partial h^2}{\partial x} = \frac{1}{\pi}\tau_x' + \frac{\epsilon'}{f'}\frac{B_u}{R_o}\frac{\partial h}{\partial y} \tag{41}$$

since $v = 0$. The more common quasi-geostrophic equations are typically integrated, in a closed basin, with the layer thickness fixed on the boundary (*e.g.* Marshall *et al.* 1988)

Figures (6–11) show successively higher Rossby numbers and the purely western boundary current of figs.(4–5) slowly transforms into a more inertial current. As the Rossby number gets higher (relative to f') the iteration scheme implicit in the correction loops evaluating the new velocities becomes less rapidly convergent. If locally the relative vorticity becomes larger than f', the iteration may diverge and the model will fail.

Figures (12 and 13) show a run where the stratification is much weaker (B_u is small). The layer thickness variations are much larger in this case, (the Rossby number and the frictional coefficient are the same as in figs.6 7) so that the ratio of thinnest to thickest values is about three. The boundary current has a significantly more inertial form than figs.(6 and 7), we comment that the layer thickness in the western boundary current is greater than one, the frictional terms are less effective, and the boundary current travels noticeably further around the boundary. As the stratification gets weaker then the layer thickness variations increase. Another effect is the slowing down of the Rossby waves. When the Burger number is small their

speed is $-B_u/f'^2$ relative to the mean flow, this is significantly slower than the value of $-1/(k^2 + B_u^{-1})$ in quasi-geostrophic models (where B_u should be nearly 1) and $-1/k^2$ in a barotropic non-divergent model. The spin-up to steady state, which depends upon these Rossby waves, may take several years even without eddies. It is this long spin-up time which makes isopycnal models with weak stratification take much longer to spin-up than their quasi-geostrophic counterparts.

In the extreme case the thickness reaches zero. The formulation of the model presented in section 2 takes no account of this and will integrate the equations regardless. In the following section we describe the modifications required to make this model cope with this 'outcropping' without allowing negative values of layer thickness.

4 Outcropping Modifications

Here we describe modifications to our model enabling it to cope with the drying up of the single shallow water layer. This 'drying up' represents the outcropping of deeper density layers. As far as we are aware, this is the only balanced model which allows the drying up of isopycnal layers.

Other isopycnal models (*e.g.* the Bleck and Boudra 1986 model) cope with surfacing isopycnals by using the flux corrected transport scheme, applied to the continuity equation, to redistribute mass. Flux corrected transport(FCT) schemes (Boris and Book 1973, Zalesak 1979) remove the possibility of negative layer thickness by locally changing the formulation of the mass flux in the continuity equation, in those places on the grid where negative layer thicknesses (and other spurious maxima or minima) are likely to occur. The FCT scheme uses a combination of an upwind formulation, a first order accurate scheme, and a higher order formulation. The combination is chosen so that no new maxima or minima (of the final fields) are formed that did not already exist at the previous step or would not be produced by the upwind scheme alone. Since the upwind formulation has the property of being unable to create negative values of h (if the CFL criterion is satisfied) then the FCT scheme maintains

h as being positive.

Although flux corrected transport schemes are numerically robust and are frequently used in numerical modelling, they are not suitable for use with our model formulation. Where flux limiting occurs the FCT type schemes change the finite differencing. The difference scheme for each point is not chosen until the direction and strength of the final velocities are known. The predictor-corrector scheme we use is based around linearisation of the finite difference scheme and depends upon knowing the finite differencing *before* we can formulate the inversion to evaluate the final velocities. Hence the pure FCT scheme is not applicable although some of its concepts can be used to develop a scheme which allows outcropping.

The scheme we describe, evaluates the mass transports required to fully remove the residuals and adjust as few of these as possible while guaranteeing that we do not create any negative values of h^{n+1}. The final distribution of mass is as close as possible to the zero residual solution. Our scheme differs from the FCT schemes in requiring only that the new fields are non-negative.

The initial predictor stage, is treated somewhat differently from subsequently stages, we limit the full mass flux, to ensure no negative values of h are created. In subsequent stages we need limit only the change in fluxes to ensure positivity of h. The residual calculation and inversion are left unaltered.

4.1 The Flux limiting scheme

Our scheme evaluates the net flux from a box which would make the box have zero mass (for the initial predictor step this is $h^{n-1}\Delta x/2\Delta t$). If the sum of the fluxes out of this box is greater than this, then the outward fluxes are limited and this new value is used in the momentum equation. These modified fluxes must be used in the momentum equation to retain the consistency of the linearisation technique.

Generally for the initial predictor step we define, for each h gridpoint, the ratio (between 0 and 1) of *outward* fluxes that would *alone* just cause outcropping. For each h point this ratio $\alpha_{i,j}$ is given by

$$\frac{-h_{i,j}^{n-1}}{2\Delta t} + R_o\mu_{i,j}\left(\frac{\max(0,U_{i+1,j}) - \min(0,U_{i,j})}{\Delta x} + \frac{\max(0,V_{i,j+1}) - \min(0,V_{i,j})}{\Delta y}\right) = 0 \tag{42}$$

$$\tag{43}$$

and

$$\alpha_{i,j} = \min(0,\mu_{i,j}) \tag{44}$$

We limit only the outward fluxes, so these are the only fluxes included in this calculation. Inward fluxes are not adjusted because they might themselves be altered by the competing requirement that the box they leave must remain non-negative. The limited fluxes we use are,

$$U_{i,j}^L = \alpha_{i-1,j}\max(0,U_{i,j}) + \alpha_{i,j}\min(0,U_{i,j}) \tag{45}$$

$$V_{i,j}^L = \alpha_{i,j-1}\max(0,V_{i,j}) + \alpha_{i,j}\min(0,V_{i,j}) \tag{46}$$

where the relevant α is taken from the box the flux is leaving. These limited fluxes are then used to evaluate $h^\#$ and $v_g^\#$ the predicted values of h^{n+1} and v_g^{n+1} using

$$\frac{h^\# - h^{n-1}}{2\Delta t} + R_o(\delta_x U^L + \delta_y V^L) = 0 \tag{47}$$

$$\overline{h}^x\left(\frac{v_g^\# - v_g^{n-1}}{2\Delta t}\right) + U^L(R_o\delta_{2x}v_g + f') + R_o\overline{\overline{V^L}^x\delta_y v_g}^y - \overline{f'u_g}^{xy}\overline{h}^x = -\epsilon' v_g^\# + \tau_M'\tau_y' \tag{48}$$

as in the non-outcropping scheme. The residual (30) is then evaluated and δU calculated using eqs.(35–36)

4.2 Flux Limiting at subsequent Stages

At subsequent stages, after the inversions provide a change in mass fluxes δU or δV, only this flux change need be limited. Since we know that the previous values U^L

or V^L do not produce negative $h^\#$, any values of $h^\# < 0$ must result from the δU or δV increment.

For a change in mass flux δU $h^\#$ changes according to,

$$\frac{\Delta h}{2\Delta t} + R_o \delta_x \delta U = 0 \tag{49}$$

where $\Delta h =$ (Value after correction $-h^\#$). The flux limiting appropriate to this must ensure that Δh is greater than $-h^\#$ where $h^\#$ is the best previously known h.

For each trial value of $h^\#_{i,j}$ we evaluate the ratio of outward fluxes that would exactly cause outcropping, this is the $\alpha_{i,j}$ which satisfies

$$\frac{-h^\#_{i,j}}{2\Delta t} + R_o \mu_{i,j} \left(\frac{\max(0, \delta U_{i+1,j}) - \min(0, \delta U_{i,j})}{\Delta x} \right) = 0 \tag{50}$$

and

$$\alpha_{i,j} = \min(0, \mu_{i,j}) \tag{51}$$

hence the limited (change in) fluxes are evaluated using

$$\delta U^L_{i,j} = \alpha_{i-1,j} \max(0, \delta U_{i,j}) + \alpha_{i,j} \min(0, \delta U_{i,j}) \tag{52}$$

and new full fluxes calculated using

$$U^L_{i,j} = U_{i,j} + \delta U^L_{i,j} \tag{53}$$

where $U_{i,j}$ was used to produce $h^\#$ and is the best known flux from either the previous time step or iteration. We use these new limited fluxes to evaluate new values of $h^\#$ with

$$\frac{h^\#_{i,j} - h^{n-1}_{i,j}}{2\Delta t} + R_o(\delta_x U^L + \delta_y V) = 0 \tag{54}$$

A similar scheme applies for increments δV.

The same structure of iteration is used as in the non-outcropping model except for this flux-correction scheme being used to redistribute the mass. The algorithm is presented in figure (3).

Using this scheme we will not remove all of the residuals at points on the grid where flux limiting occurs. In classical problems where the equations cannot be

satisfied exactly at discontinuities, adjacent residuals are ignored. In this case it is unclear before the inversion whether the fluid will outcrop and whether the equations can be exactly satisfied at each grid box. Hence we cannot just ignore the residual at boxes which will outcrop at the inversion stage. We choose to solve the exact equations in the inversions and modify the fluxes and residuals afterwards. Since the flux limiting adjusts fluxes, some non-zero residuals are inevitable. In practice if we leave these residuals non-zero they grow and ultimately cause model failure. We circumvent this difficulty by making use of our balance condition ($v_g = g'\delta_x h/f$) to evaluate v_g^{n+1} near flux limited points after the rest of the step has been completed.

Near flux limited points the geostrophic flow is not obtained by the prognostic integration, of the momentum equations. Although this scheme leads to the best value of mass transport consistent with non-negative layer thickness, and hence the best possible distribution of mass, the exact balances at the outcrop edge are not necessarily consistent with the momentum equations. The exact quadratic momentum flux conservation is lost at the outcrop edge. A similar problem is discussed by Bleck and Boudra (1986).

5 Solutions with Outcropping

In this section we show solutions from our outcropping model. We first reproduce a known result. We configure the model to compare solutions both with the numerical results of Bogue, Huang and Bryan(1986)(hereafter BHB) and the analytic solutions of Parsons(1969). The wind forcing is purely zonal ($\tau_x = -\tau_0 cos(\pi y/L), \tau_y = 0$), and the non-dimensional parameters are ($3.1\text{x}10^{-4}, 1.64\text{x}10^{-4}, 2.\text{x}10^{-2}, 1.4$) respectively for R_o, B_u, ϵ' and γ. These correspond to inertial and frictional length scales of 1/57 and 1/50 of the basin respectively.

The BHB model integrates the shallow water equations forward in time, omitting the non-linear advection terms and the time-derivative term in each momentum equation. They use a linear drag frictional dissipation. If there is a unique steady state then in the limit of small Rossby number, solutions to our model (which includes

momentum advection) should coincide with those of BHB (although in their model friction acts on the full velocity and in ours on the geostrophic velocity).

Fig.(14) shows the (non-dimensional) layer thickness from our model. The parameters (see table 1) are set up to reproduce figure (1b) of BHB (our fig. 15). This solution has a low Rossby number but has a large outcropped region in the north-west corner of the basin, south of which is the separated boundary current representing the Gulf stream.

In our solution the minimum layer thickness is exactly zero suggesting that our flux limiting scheme is accurately maintaining the non-negative nature of the fields. Over much of the outcropped region the layer thickness is of order 10^{-3} relative to the mean (which is 1). The thin lines represent the analytic solution obtained by finding the Parsons solution with the same Rossby and Burger numbers.

There is a very good agreement between our solution and BHB's. The outcrop line follows a very similar path, by looking at the layer thickness numbers directly from our model we can see the 0.3 contour hits the north and west walls at the same point to within 2 gridpoints. We find our maximum layer thickness is 1.89 in the centre of the gyre, and in figure (15) it looks very similar. We note a substantially smaller outcrop area on these numerical solutions compared with the analytic solution. This is consistent with the analytic solutions' higher maximum thickness of 2.36. The layer thickness on the eastern wall (h'_e) is 0.55 in the analytic solution and varies between about 0.5 and 0.6 in our model. We note that these numerical solutions have relatively high friction and so layer thickness contours intersect the eastern wall. The close agreement between our model and that of BHB leads us to believe the model is accurately reproducing the numerical solution.

Figure(16) is a run with twice the inertial length scale twice the Rossby radius and half the frictional length scale of figure(14). The analytic solution depends only on one parameter which Parsons calls λ. In our notation this is $R_o/\pi B_u$. The analytic solutions corresponding to the parameters in figures (14) and (16) are the same.

The most noticeable differences are in the overshoot, the separation of the jet from the western wall is no longer a smooth right hand turn into the basin. Rather the fluid overshoots the smooth separation latitude, dissipating vorticity (via friction) until it can smoothly plunge south again to rejoin the mostly inertialess separated jet. In this solution the layer thickness minimum is about $-2\text{x}10^{-3}$ and the maximum is 2.02 times the mean thickness. will The analytic solution is again shown in thin lined contours.

We have been unable to obtain solutions with a significantly higher Rossby number, due to divergence of the iteration scheme. A future paper will examine solutions with higher inertia where the Parsons solution is not valid.

5.1 Discussion

In this paper we have built an ocean model based upon the geostrophic momentum equations. We believe this model to be the first balanced model to allow drying up of shallow water layers. It has been found to be both robust in its numerical formulation and versatile in its applications and has been able to reproduce classical results of idealised gyre theory. This balanced model is able to examine solutions where large layer thickness variations and high inertial non-linearity are both included. Our model uses linear drag dissipation, a shallow water model with gravity waves included would almost certainly need higher order dissipative forms providing a sink of enstrophy on the grid scale, to aid numerical stability (Sadourney 1975).

We have found the model time step to be limited by a Kelvin wave which may propagate at angular frequencies up to the Coriolis parameter. It is important to note that these Kelvin waves are not gravity waves in any sense, they are geostrophic in both directions in contrast to shallow water and primitive equation Kelvin waves. Kelvin waves are known to be present in other balanced models, where the boundary conditions allow a normal geostrophic velocity at boundaries(Gent and McWilliams 1983).

Although there is guaranteed to be a unique solution to the continuous semi-

geostrophic equations (on an f-plane) with all non-negative mass (Cullen and Purser 1989) the unique solution to the finite difference equations can, at times, involve negative layer thickness. As the Rossby number increases, the source/sink of momentum implied by the imposition of geostrophy at outcropped points may have a larger effect on the interior flow. A better condition upon the geostrophic velocity at the outcrop edge is clearly required.

Further enhancements to the model are envisaged with a wider range of applicability. These include a more robust solution technique involving solving for δU and δV simultaneously, a many layer version, coastlines and diabatic forcing. Future papers studying outcropping solutions with large inertial effects are in preparation.

Acknowledgments

John Marshall participated in many useful discussions throughout this work and his help is gratefully acknowledged. PC was supported by NERC, the UK Meteorological Office and UCAR during this work.

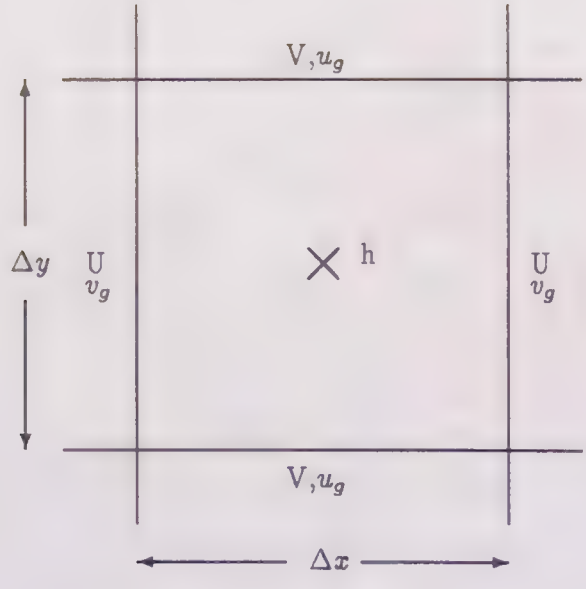

Figure 1: Arrangement of Variables on the Grid

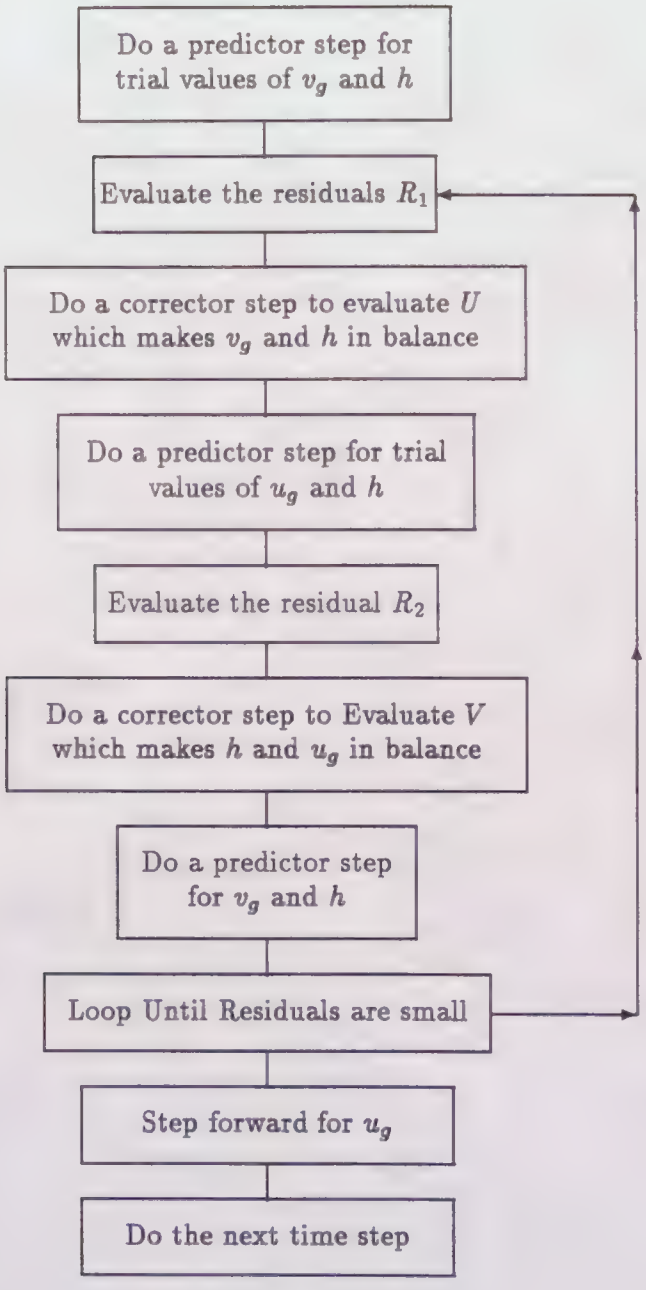

Figure 2: Algorithm for non-outcropping code.

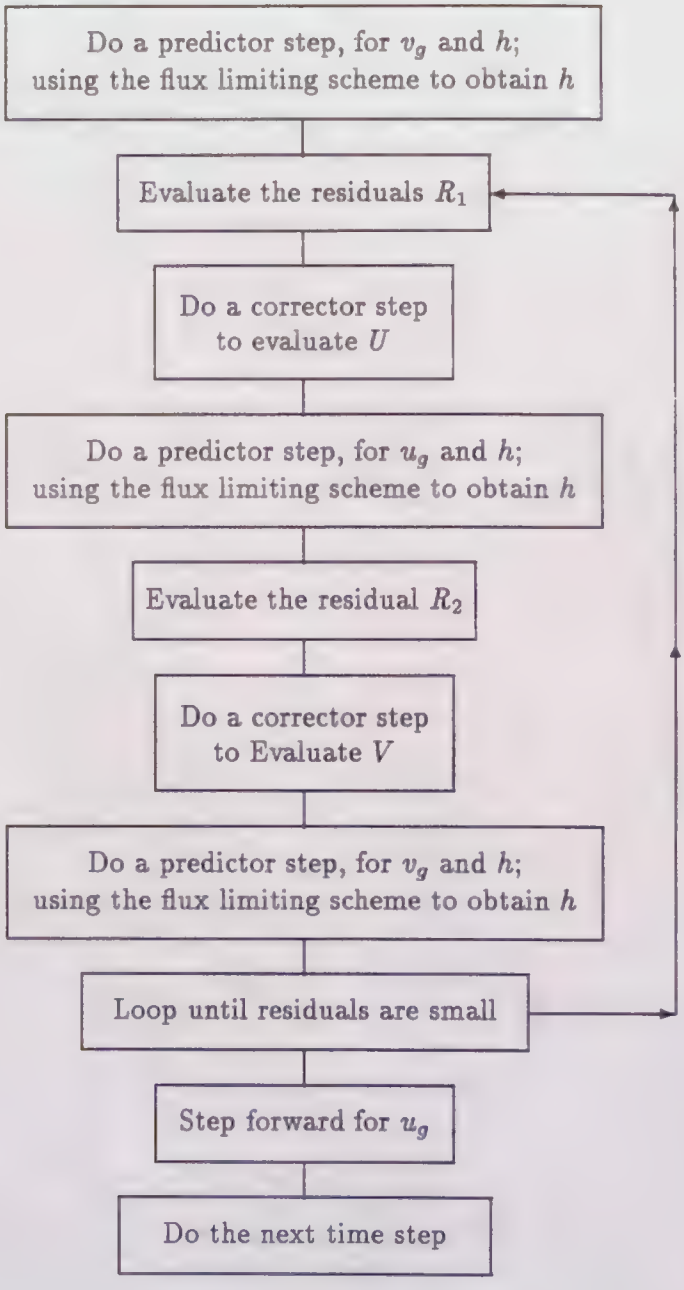

Figure 3: Algorithm for outcropping code.

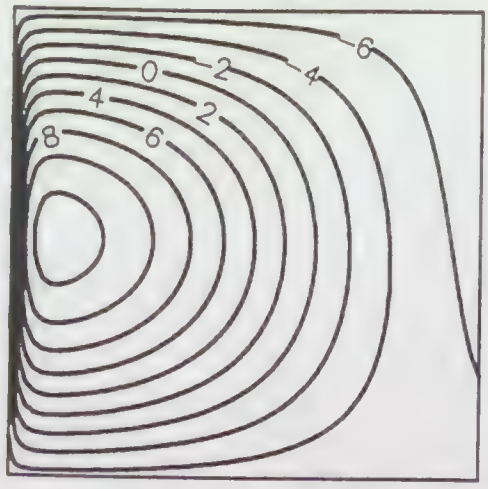

Figure 4: **Layer thickness perturbation $(h-1)$ from our model. The contour interval is $2\text{x}10^{-9}$. The solution is reminiscent of the Stommel(1948) solution. Note that the contours intersect the boundary. The parameters are given in fig. 17**

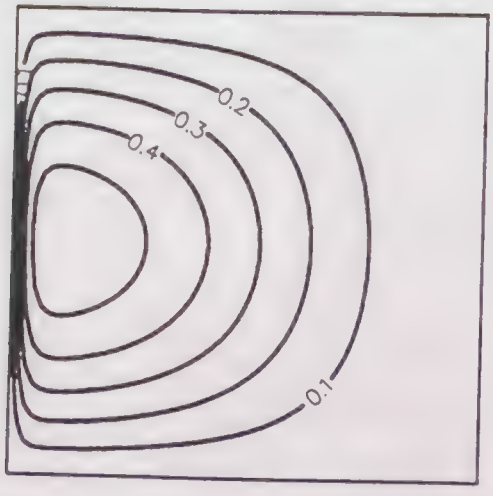

Figure 5: **Streamlines from our model. Parameters are the same as in fig. 4. Here the streamlines do not intersect the walls. The contour interval is 0.2.**

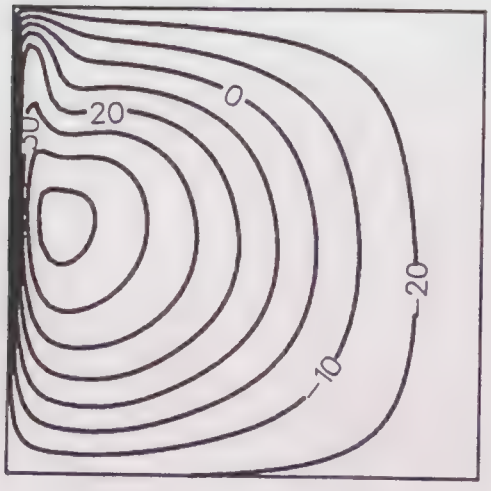

Figure 6: **Layer thickness perturbation from our model. With a higher Rossby number** ($4\text{x}10^{-4}$), **hence higher inertia, the purely western boundary current of figures 4 and 5 is replaced with a flow of significant north-south asymmetry. The contour interval is** $1.0\text{x}10^{-6}$.

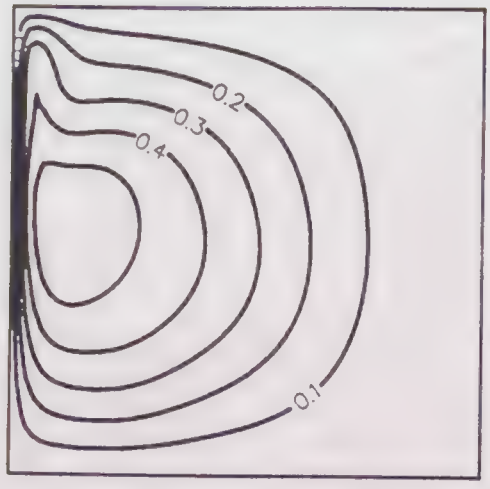

Figure 7: **Streamlines corresponding of the run fo fig. 6. The parameters are as in figure 6.**

Figure 8: **Layer thickness perturbations with yet higher Rossby number ($1x10^{-3}$). The contour interval is $2.5x10^{-6}$. The boundary current is both frictional and inertial here.**

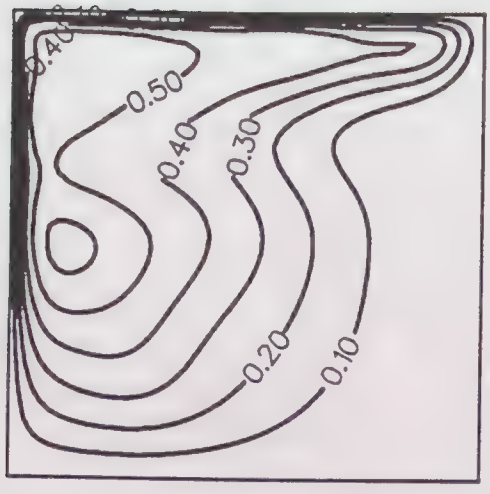

Figure 9: **Streamlines corresponding to figure 8.**

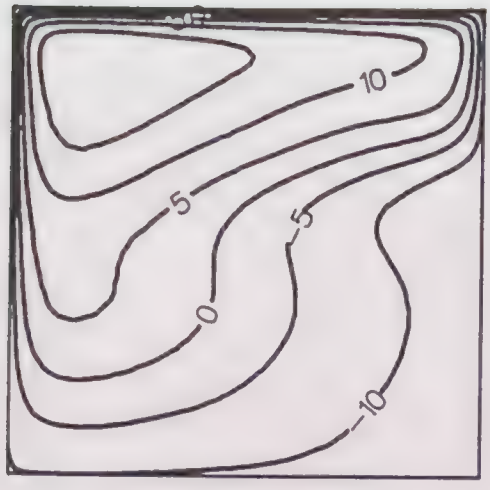

Figure 10: **Layer thickness perturbations. Here the friction is decreased relative to figures 8 and 9 and the western boundary current has been almost entirely replaced by a northern current. The contour interval is** 1.0×10^{-6}.

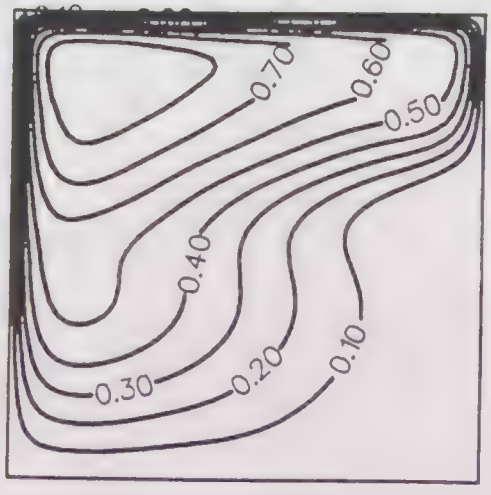

Figure 11: **Streamlines corresponding to figure 10. Note the different pattern compared to figure 10. This is especially noticeable near the southern wall, where the streamlines do not intersect the wall.**

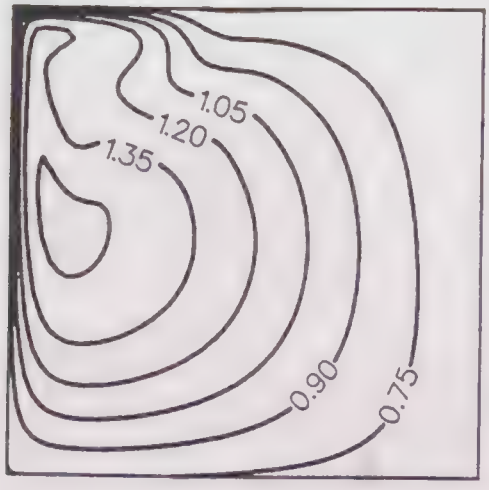

Figure 12: **Layer thickness from a run with large thickness variations. The contour interval is 0.15. The parameters (see fig. 17, table 1) are the same is for figures 6 and 7 except for the much lower Burger number.**

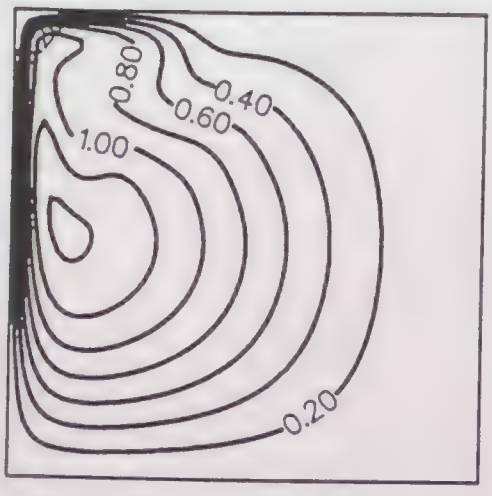

Figure 13: **Streamlines corresponding to figure 12**

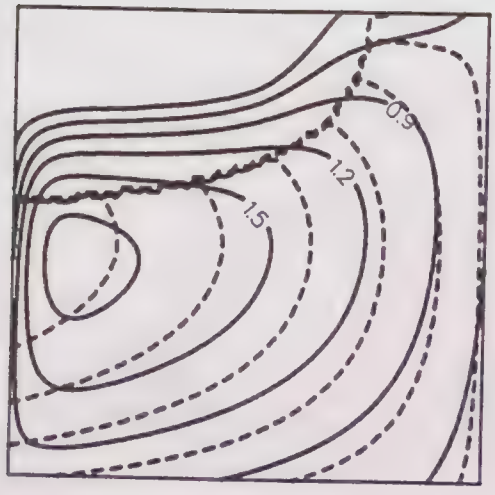

Figure 14: **Layer thickness from the outcropping version of our model. The parameters are the same as for fig. 1b of BHB (see also table 1). Continuous lines are from our model, dashed lines are the analytic solution. The contour interval is 0.3 for both plots.**

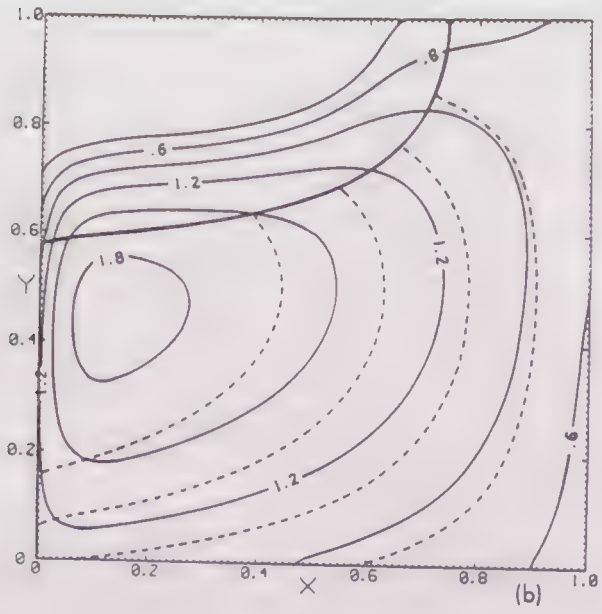

Figure 15: **The layer thickness from Bogue et al. (1986,fig. 1b). The solid line is the analytic outcrop line, and the dashed lines are analytic pressure contours. The contour interval is 0.3. Parameters are exactly the same as in figure 14**

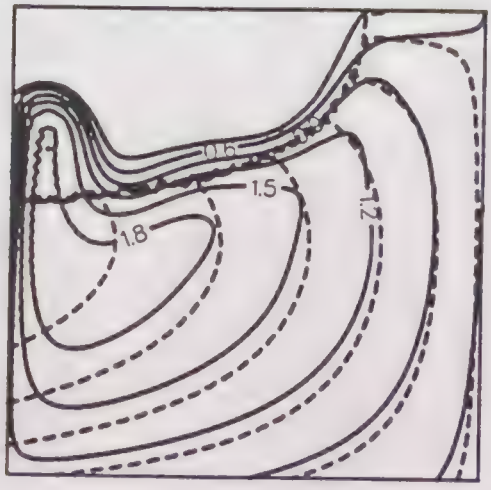

Figure 16: **Layer thickness from the outcropping version of our model. Continuous lines are from our model, dashed lines are the analytic solution. Here the inertial length scale is well resolved and the boundary current is clearly overshooting. The contour interval is 0.3 for both plots. Linear theory suggest that the solution will be the same as in figures 14 and 15.**

Figure Numbers	*Parameters*		
	R_o	B_u	ϵ'
4,5	$1.0\text{x}10^{-6}$	100	$2.0\text{x}10^{-2}$
6,7	$4.0\text{x}10^{-4}$	100	$2.0\text{x}10^{-2}$
8,9	$1.0\text{x}10^{-3}$	100	$1.0\text{x}10^{-2}$
10,11	$1.0\text{x}10^{-3}$	100	$8.0\text{x}10^{-3}$
12,13	$4.0\text{x}10^{-4}$	100	$2.0\text{x}10^{-2}$
14	$3.1\text{x}10^{-4}$	$1.64\text{x}10^{-4}$	$6.0\text{x}10^{-2}$
16	$1.23\text{x}10^{-3}$	$6.56\text{x}10^{-4}$	$3.0\text{x}10^{-2}$

Figure 17: Table 1: Relating Figure Numbers to Parameters.

Allen, J.S., J.A. Barth and P.A. Newburger, 1990: On Intermediate Models for Barotropic Continental Shelf and Slope Flow Fields: Part I, Formulation and Comparison of Exact Solutions *J. Phys. Oceanogr.*, **20**, 1017–1042.

Asselin, R., 1972: Frequency Filter for Time Integrations *Mon. Wea. Rev.*, **100**, 487-490.

Arakawa, A., 1972: Design of the UCLA general Circulation Model *Numerical Simulation of Weather and Climate,Dept. of Meteorology, Univ. of Calif.,Los Angeles*, **Tech. Rept. 7**, 116pp.

Barth, J.A., J.S. Allen and P.A. Newburger, 1990: On Intermediate Models for Barotropic Continental Shelf and Slope Flow Fields: Part II, Comparison of Numerical Model Solutions in Doubly-Periodic Domains. *J. Phys. Oceanogr.*, **20**, 1017–1042.

Bleck, R. and D.B.Boudra, 1986: Wind-driven spin-up in eddy-resolving ocean models formulated in isopycnic and isobaric coordinates. *J.Geophys.Res.*, **91C**, 7611–7621.

Bogue, N.M.,R.X. Huang and K.Bryan, 1986: Verification experiments with an isopycnal coordinate ocean model *J. Phys. Oceanogr.*, **16**, 985-990.

Boris J.P. and D.L. Book, (1973): Flux-corrected transport, 1.SHASTA,A fluid transport Algorithm that works *J.Comp.Phys.*, **11**, 388–69.

Cloke, P., 1992: Semi-Geostrophic Ocean Modelling *PhD Thesis for the Imperial College of the Univ. of London*, , .

Cullen, M.J.P., 1989a: Implicit Finite Difference Methods for Modelling Discontinuous Atmospheric Flows *J. Comp. Phys.*, **81**, 319–348.

Cullen, M.J.P., 1989b: On the Incorporation of Atmospheric Boundary Layer Effects into a Balanced Model *Quart. J. R. Met. Soc.*, **115**, 1109–1131.

Cullen M.J.P. and R.J. Purser, 1989: Properties of the Lagrangian Semigeostrophic Equations *J.Atmos. Sci.*, **46**, 2684–2697.

Eliassen A., 1948: The Quasi-static Equations of Motion with Pressure as Independent Variable. *Geophys. Publ.*, **17(3)**, .

Gent,P.R. and J.C.McWilliams, 1983: Consistent balanced models in bounded a nd periodic domains. *Dyn.Atmos.ocean*, **7**, 67–93.

Hoskins,B.J., 1975: The gesotrophic momentum approximation and the semi-geostrophic equations *Journ.Atmos.Sci*, **32**, 233–242.

Magnusdottir, G. and W.G. Schubert, 1990: The Generalization of Semigeostrophic Theory to a β-plane. *J. Atmos. Sci.*, **47**, 1714–1720.

McWilliams, J.C. and P.R. Gent, 1980: Intermediate models of planetary circulations in atmosphere and ocean. *J. Atmos. Sci.*, **37**, 1657–1678.

McWilliams, J.C., N.J. Norton, P.R. Gent and D.B.Haidvogel, 1990: A Linear Balance Model of Wind-driven Mid-lattitude ocean Circulation. *J. Phys. Oceanogr.*, **20**, 1349–1378.

Parsons, A.T., 1969: A Two-Layer Model of Gulf Stream Separation. *J.Fluid Mech.*, **39**, 511–528.

Robert, A.J., 1966: The Integration of a Low Order Spectral Form of the Primitive Meteorological Equations *J. Met. Soc. Japan, Ser 2*, **44**, 237–245.

Salmon, R., 1983: Practical use of Hamilton's Principle *J.Fluid Mech.*, **132**, 431–444.

Salmon R., 1985: New Equations for Nearly geostrophic flow. *J.Fluid Mech.*, **153**, 461–477.

Shutts, G.J., 1989: Planetary Semi-Geostrophic Equations Derived from Hamilton's Principle *J. Fluid. Mech.*, **208**, 545–573.

Sadourney R., 1975: The Dynamics of Finite Difference models of the Shallow Water Equations *J.Atmos.Sci.*, **32**, 680–689.

Stommel, H., 1948: The Westward Intensification of WInd-driven ocean currents. *Trans. Amer. Geophys. Union*, **99**, 202–206.

Veronis, G., 1966: Wind-driven Ocean Circulation–Part 2. Numerical Solutions of the non-linear problem. *Deep-Sea Res.*, **13**, 31–55.

Williams G.P., 1969: Numerical intergation of the Three-dimensional Navier-Stokes equations for Incompressible flow. *J. Fluid. Mech.*, **37**, 727-750.

Zalesak S.T., 1979: Fully multidimensional flux-corrected transport algorithms for fluids. *J.Comp.Phys*, **31**, 335–362.